J. Fluid Mech. (2019), *vol.* 867, *pp.* 195–215.
doi:10.1017/jfm.2019.116

Cascades of temperature and entropy fluctuations in compressible turbulence

Jianchun Wang[1,†], Minping Wan[1,†], Song Chen[1], Chenyue Xie[1], Lian-Ping Wang[1,2] and Shiyi Chen[1,3]

[1]Department of Mechanics and Aerospace Engineering, Southern University of Science and Technology, Shenzhen, Guangdong 518055, PR China

[2]Department of Mechanical Engineering, University of Delaware, Newark, DE 19716, USA

[3]State Key Laboratory of Turbulence and Complex Systems, Center for Applied Physics and Technology, College of Engineering, Peking University, Beijing 100871, PR China

(Received 7 October 2018; revised 24 December 2018; accepted 1 February 2019; first published online 20 March 2019)

Cascades of temperature and entropy fluctuations are studied by numerical simulations of stationary three-dimensional compressible turbulence with a heat source. The fluctuation spectra of velocity, compressible velocity component, density and pressure exhibit the $-5/3$ scaling in an inertial range. The strong acoustic equilibrium relation between spectra of the compressible velocity component and pressure is observed. The $-5/3$ scaling behaviour is also identified for the fluctuation spectra of temperature and entropy, with the Obukhov–Corrsin constants close to that of a passive scalar spectrum. It is shown by Kovasznay decomposition that the dynamics of the temperature field is dominated by the entropic mode. The average subgrid-scale (SGS) fluxes of temperature and entropy normalized by the total dissipation rates are close to 1 in the inertial range. The cascade of temperature is dominated by the compressible mode of the velocity field, indicating that the theory of a passive scalar in incompressible turbulence is not suitable to describe the inter-scale transfer of temperature in compressible turbulence. In contrast, the cascade of entropy is dominated by the solenoidal mode of the velocity field. The different behaviours of cascades of temperature and entropy are partly explained by the geometrical properties of SGS fluxes. Moreover, the different effects of local compressibility on the SGS fluxes of temperature and entropy are investigated by conditional averaging with respect to the filtered dilatation, demonstrating that the effect of compressibility on the cascade of temperature is much stronger than on the cascade of entropy.

Key words: compressible turbulence, isotropic turbulence

1. Introduction

Heat transport in compressible turbulence plays an important role in many natural phenomena and industrial applications, including supersonic combustion, the design of hypersonic aircraft and star formation in astrophysics. Recently, there have been

† Email addresses for correspondence: wangjc@sustech.edu.cn, wanmp@sustech.edu.cn

a number of studies on the spectra and inter-scale transfer of kinetic energy in three-dimensional compressible turbulence (Falkovich, Fouxon & Oz 2010; Aluie 2011; Galtier & Banerjee 2011; Suman & Girimaji 2011; Aluie, Li & Li 2012; Wagner *et al.* 2012; Aluie 2013; Kritsuk, Wagner & Norman 2013; Wang *et al.* 2013; Jagannathan & Donzis 2016; Livescu & Li 2017; Eyink & Drivas 2018; Wang *et al.* 2018*a*,*b*), which extended the traditional Richardson–Kolmogorov–Onsager picture of kinetic energy cascade (Frisch 1995; Cardy, Falkovich & Gawedzki 2008; Sagaut & Cambon 2008) to compressible turbulence. In contrast, the properties of inter-scale transfer of heat and entropy are much less understood as compared to those of kinetic energy transfer in compressible turbulence.

Zank & Matthaeus (1990, 1991) made a theoretical analysis on the two distinct states of weakly compressible turbulence: in the heat-fluctuation-dominated state, due to the effect of heat source, the classical passive scalar equation for temperature is recovered; in the heat-fluctuation-modified state, the temperature fluctuation is related to the acoustic mode or pseudo-sound mode. By an asymptotic analysis, Bayly, Levermore & Passot (1992) predicted that temperature, entropy and density have $k^{-5/3}$ power spectra in the inertial range of weakly compressible turbulent flows with some heat source. Wang, Gotoh & Watanabe (2017) performed numerical simulations of solenoidally forced compressible isotropic turbulence without any heat source at turbulent Mach numbers, M_t, from 0.05 to 1.0. The spectra of pressure, density and temperature exhibit a $k^{-7/3}$ scaling for $M_t \leqslant 0.3$ and a $k^{-5/3}$ scaling for $0.5 \leqslant M_t \leqslant 1.0$. A theoretical analysis by Drivas & Eyink (2018), Eyink & Drivas (2018) showed that entropy conservation anomalies occur in compressible turbulence via two mechanisms: an anomalous input of negative entropy by pressure work and a cascade of negative entropy to small scales.

In this study, we discuss the spectra and inter-scale transfer of temperature and entropy fluctuations in numerical simulations of compressible turbulence, with a specific focus on the effect of compression and expansion motions on the fluxes of temperature and entropy. The rest of the paper is organized as follows. In § 2, we describe the governing equations and computational method. In § 3, we provide the one-point statistics of velocity and thermodynamic variables in the numerical simulations. In § 4, we study the spectra of velocity, density, pressure, temperature and entropy. In § 5, we investigate the inter-scale transfer of temperature and entropy fluctuations. In § 6, we present some discussions about the statistics and inter-scale transfer of temperature and entropy fluctuations. Finally, conclusions will be given in § 7.

2. Governing equations and numerical method

The following dimensionless Navier–Stokes equations in conservative form are solved numerically in this study (Wang *et al.* 2010, 2018*a*)

$$\frac{\partial \rho}{\partial t} + \frac{\partial (\rho u_j)}{\partial x_j} = 0, \tag{2.1}$$

$$\frac{\partial (\rho u_i)}{\partial t} + \frac{\partial [\rho u_i u_j + p\delta_{ij}]}{\partial x_j} = \frac{1}{Re}\frac{\partial \sigma_{ij}}{\partial x_j} + \mathcal{F}_i, \tag{2.2}$$

$$\frac{\partial \mathcal{E}}{\partial t} + \frac{\partial [(\mathcal{E}+p)u_j]}{\partial x_j} = \frac{1}{\alpha}\frac{\partial}{\partial x_j}\left(\kappa \frac{\partial T}{\partial x_j}\right) + \frac{1}{Re}\frac{\partial (\sigma_{ij}u_i)}{\partial x_j} - \Lambda + \mathcal{F}_I + \mathcal{F}_j u_j, \tag{2.3}$$

$$p = \rho T/(\gamma M^2), \tag{2.4}$$

where ρ is the density, u_i is the velocity component, p is the pressure and T is the temperature. The viscous stress σ_{ij} is defined by

$$\sigma_{ij} = \mu\left(\frac{\partial u_i}{\partial x_j} + \frac{\partial u_j}{\partial x_i}\right) - \frac{2}{3}\mu\theta\delta_{ij}, \tag{2.5}$$

where, $\theta = \partial u_k/\partial x_k$ is the normalized velocity divergence; $\mathcal{F}_i$ is a large-scale forcing to the fluid momentum, $\mathcal{F}_I$ is a large-scale forcing to the internal energy and Λ is a large-scale cooling function per unit volume. The total energy per unit volume $\mathcal{E}$ is defined by

$$\mathcal{E} = \frac{p}{\gamma - 1} + \frac{1}{2}\rho(u_j u_j). \tag{2.6}$$

A set of reference scales can be introduced to normalize the hydrodynamic and thermodynamic variables in compressible turbulence, including the reference length L_f, velocity U_f, density ρ_f, pressure $p_f = \rho_f U_f^2$, temperature T_f, energy per unit volume $\rho_f U_f^2$, viscosity μ_f and thermal conductivity κ_f respectively. After normalization, three reference governing parameters are obtained: the reference Reynolds number $Re \equiv \rho_f U_f L_f/\mu_f$, the reference Mach number $M = U_f/c_f$ and the reference Prandtl number $Pr \equiv \mu_f C_p/\kappa_f$. Here, the speed of sound is defined by $c_f \equiv \sqrt{\gamma R T_f}$; $\gamma \equiv C_p/C_v$ is the ratio of specific heat at constant pressure C_p to that at constant volume C_v, which is assumed to be equal to 1.4, R is the specific gas constant. The parameter α is defined by $\alpha \equiv Pr\,Re(\gamma - 1)M^2$. It is assumed that the parameter Pr is equal to 0.7.

We apply Sutherland's law for the non-dimensional temperature-dependent viscosity coefficient μ and thermal conductivity coefficient κ (Wang *et al.* 2010). We apply large-scale forcing to the solenoidal velocity component and internal energy by fixing the spectrum within the two lowest wavenumber shells (Chen & Cao 1997; Wang *et al.* 2010; Donzis & Maqui 2016). We also employ a uniform thermal cooling Λ to sustain the internal energy in a statistically steady state (Wang *et al.* 2010).

We utilize a hybrid numerical method (Wang *et al.* 2010) to simulate stationary three-dimensional compressible isotropic turbulence with a heat source in a cubic box at a 1024^3 grid resolution. The hybrid scheme combines an eighth-order compact finite difference scheme (Lele 1992) for smooth regions and a seventh-order weighted essentially non-oscillatory (WENO) scheme (Balsara & Shu 2000) for shock regions. Some grid refinement studies of the hybrid scheme for a turbulent Mach number around 1.0 were performed in previous works (Wang *et al.* 2011, 2012).

The dynamical equation of temperature T can be derived as (Sagaut & Cambon 2008; Wang *et al.* 2017):

$$\frac{\partial T}{\partial t} + u_j\frac{\partial T}{\partial x_j} = -(\gamma - 1)T\theta + D_\kappa + D_\mu + f_T, \tag{2.7}$$

where the thermal diffusion term D_κ and the viscous dissipation term D_μ are given by $D_\kappa = (1/\rho c_v)(\partial/\partial x_j)(\kappa(\partial T/\partial x_j))$ and $D_\mu = (1/Re)(\sigma_{ij}/\rho c_v)(\partial u_i/\partial x_j)$, respectively. Here $c_v = 1/(\gamma(\gamma - 1)M^2)$. The effect of large-scale forcing is represented by f_T.

Temperature can be decomposed into a spatially averaged value T_0 and a fluctuating value T_1: $T = T_0 + T_1$, where $T_0 = \langle T\rangle$. The equation for the root-mean-square (r.m.s.) value of temperature can be written as:

$$\frac{\partial}{\partial t}\langle T_1^2\rangle = \epsilon_T^{inj} - \epsilon_T, \tag{2.8}$$

Resolution	Re_λ	M_t	$\eta/\Delta x$	u'	u^S_{rms}	u^C_{rms}	ϵ_K
1024^3	247	0.20	1.07	2.31	2.16	0.81	0.68
1024^3	257	0.60	1.09	2.28	2.22	0.52	0.62

TABLE 1. Simulation parameters and resulting flow statistics.

where, the total dissipation rate of temperature is $\epsilon_T = \epsilon_T^\theta + \epsilon_T^\kappa + \epsilon_T^\mu$. The dissipation rates due to dilatation, thermal diffusion and viscous dissipation are, respectively, $\epsilon_T^\theta = -(3-2\gamma)\langle T_1^2\theta\rangle + 2(\gamma-1)T_0\langle T_1\theta\rangle$, $\epsilon_T^\kappa = 2\langle\kappa(\partial T_1/\partial x_j)(\partial/\partial x_j)(T_1/\rho c_v)\rangle$ and $\epsilon_T^\mu = -2\langle(1/Re)(T_1\sigma_{ij}/\rho c_v)(\partial u_i/\partial x_j)\rangle$; $\epsilon_T^{inj} = 2\langle T_1 f_T\rangle$ represents the injection of temperature fluctuations by large-scale forcing.

The dynamical equation for the dimensionless entropy per unit mass $s = \log(T/\rho^{\gamma-1})$ can be readily derived as (Bayly *et al.* 1992; Eyink & Drivas 2018):

$$\frac{\partial s}{\partial t} + u_j\frac{\partial s}{\partial x_j} = \frac{1}{T}D_\kappa + \frac{1}{T}D_\mu + \frac{1}{T}f_T. \tag{2.9}$$

Equation (2.9) is similar to the passive scalar transport equation. The equation for the r.m.s. value of entropy can be written as:

$$\frac{\partial}{\partial t}\langle(s_1)^2\rangle = \epsilon_s^{inj} - \epsilon_s, \tag{2.10}$$

where, $s_1 = s - s_0$, $s_0 = \langle s\rangle$ and the total dissipation rate of entropy is $\epsilon_s = \epsilon_s^\theta + \epsilon_s^\kappa + \epsilon_s^\mu$. The dissipation rates due to dilatation, thermal diffusion and viscous dissipation are, respectively, $\epsilon_s^\theta = -\langle s_1^2\theta\rangle$, $\epsilon_s^\kappa = 2\langle\kappa(\partial T/\partial x_j)(\partial/\partial x_j)(s_1/c_v\rho T)\rangle$ and $\epsilon_s^\mu = -2\langle(1/Re)(s_1\sigma_{ij}/c_v\rho T)(\partial u_i/\partial x_j)\rangle$; $\epsilon_s^{inj} = 2\langle s_1 f_T/T\rangle$ represents the injection of entropy fluctuations by large-scale forcing.

3. One-point statistics of compressible turbulence

Overall statistics for simulated compressible turbulent flows are given in table 1. The Taylor microscale Reynolds number Re_λ and the turbulent Mach number M_t are defined, respectively by (Wang *et al.* 2018*a*)

$$Re_\lambda = Re\frac{\langle\rho\rangle u'\lambda}{\sqrt{3}\langle\mu\rangle}, \quad M_t = M\frac{u'}{\langle\sqrt{T}\rangle}, \tag{3.1a,b}$$

where $\langle\,\rangle$ stands for spatial average. The r.m.s. velocity magnitude is $u' = \sqrt{\langle u_1^2+u_2^2+u_3^2\rangle}$ and the Taylor microscale is

$$\lambda = \sqrt{\frac{\langle u_1^2+u_2^2+u_3^2\rangle}{\langle(\partial u_1/\partial x_1)^2+(\partial u_2/\partial x_2)^2+(\partial u_3/\partial x_3)^2\rangle}}. \tag{3.2}$$

The Taylor Reynolds numbers Re_λ are close to 250 in the numerical simulations. Two turbulent Mach numbers are considered: $M_t = 0.2$ and $M_t = 0.6$.

The Kolmogorov length scale η of compressible turbulence is defined by (Wang *et al.* 2018*a*)

$$\eta = [\langle\mu/(Re\,\rho)\rangle^3/\epsilon]^{1/4}, \tag{3.3}$$

M_t	p_0	T_0	s_0	p_{rms}/p_0	ρ_{rms}/ρ_0	T_{rms}/T_0	s_{rms}	$\sqrt{\gamma\rho_0 p_0}u^C_{rms}/p_{rms}$
0.20	92.0	1.02	0.02	0.10	0.18	0.16	0.22	1.00
0.60	10.2	1.02	0.02	0.21	0.21	0.16	0.20	0.92

TABLE 2. Statistics of thermodynamic variables.

where ϵ is the spatial average of the viscous dissipation rate of kinetic energy per unit mass:

$$\epsilon = \frac{1}{\langle\rho\rangle}\left\langle\frac{\sigma_{ij}S_{ij}}{Re}\right\rangle. \tag{3.4}$$

The resolution parameter $\eta/\Delta x$ is in the range $1.07 \leqslant \eta/\Delta x \leqslant 1.09$ in the numerical simulations, where Δx denotes the grid length in each direction. Consequently, the resolution parameter $k_{max}\eta$ is in the range $3.36 \leqslant k_{max}\eta \leqslant 3.42$, where the largest wavenumber k_{max} is half of the number of grids N in each direction: $k_{max} = N/2 = \pi/\Delta x$. Previous grid refinement studies showed that grid resolutions $k_{max}\eta \geqslant 3.3$ are enough for the convergence of flow statistics, including the kinetic energy spectrum at different wavenumbers and the probability density functions (PDFs) of velocity divergence and vorticity (Wang *et al.* 2011, 2012).

By applying the Helmholtz decomposition, we decompose the velocity field $\boldsymbol{u}$ into a solenoidal component $\boldsymbol{u}^S$ and a compressible component $\boldsymbol{u}^C$ (Samtaney, Pullin & Kosovic 2001; Sagaut & Cambon 2008; Wang *et al.* 2012):

$$\boldsymbol{u} = \boldsymbol{u}^S + \boldsymbol{u}^C, \tag{3.5}$$

where $\boldsymbol{\nabla}\cdot\boldsymbol{u}^S = 0$ and $\boldsymbol{\nabla}\times\boldsymbol{u}^C = 0$. The r.m.s. values of the solenoidal and compressible velocity components are defined by $u^S_{rms} = \sqrt{\langle(u^S_1)^2 + (u^S_2)^2 + (u^S_3)^2\rangle}$ and $u^C_{rms} = \sqrt{\langle(u^C_1)^2 + (u^C_2)^2 + (u^C_3)^2\rangle}$, respectively. It is shown that u^S_{rms} is close to u', while u^C_{rms} is significantly smaller than u^S_{rms}, implying that the solenoidal velocity component is predominant over its compressible counterpart.

The total dissipation rate of kinetic energy per unit mass is given by

$$\epsilon_K = \frac{1}{\langle\rho\rangle}\left[-\langle p\theta\rangle + \left\langle\frac{\sigma_{ij}S_{ij}}{Re}\right\rangle\right], \tag{3.6}$$

namely, the total conversion rate of kinetic energy into internal energy by the pressure dilatation $-\langle p\theta\rangle/\langle\rho\rangle$ and the viscous dissipation ϵ. It is found that the magnitude of $-\langle p\theta\rangle/\langle\rho\rangle$ is much smaller than that of ϵ, and the value of ϵ is very close to that of ϵ_K.

The dimensionless entropy is given by $s = \log(T/\rho^{\gamma-1})$. The average values of pressure, density, temperature and entropy are given by $p_0 = \langle p\rangle$, $\rho_0 = \langle\rho\rangle$, $T_0 = \langle T\rangle$, $s_0 = \langle s\rangle$. The average density is $\rho_0 = 1$ in the numerical simulations. The r.m.s. values of pressure, density, temperature and entropy are defined by: $p_{rms} = \sqrt{\langle(p-p_0)^2\rangle}$, $\rho_{rms} = \sqrt{\langle(\rho-\rho_0)^2\rangle}$, $T_{rms} = \sqrt{\langle(T-T_0)^2\rangle}$ and $s_{rms} = \sqrt{\langle(s-s_0)^2\rangle}$, respectively. The one-point statistics of thermodynamic variables are given in table 2. We observe that p_{rms}/p_0 increases rapidly with the turbulent Mach number, while ρ_{rms}/ρ_0, T_{rms}/T_0 and s_{rms} are insensitive to the change of turbulent Mach number. Previous studies showed that if the compressible velocity component is dominated by acoustic waves, there are

equipartition relations between pressure and the compressible velocity component in weak and strong forms (Sarkar *et al.* 1991; Sagaut & Cambon 2008; Jagannathan & Donzis 2016; Wang *et al.* 2017; Chen *et al.* 2018; Wang *et al.* 2018*b*). The weak acoustic equilibrium can be expressed as

$$p_{rms} \approx \rho_0 c_0 u^C_{rms}, \tag{3.7}$$

where, $c_0 = \sqrt{\gamma p_0/\rho_0}$ is the speed of sound. The above relation is equivalent to

$$\frac{\sqrt{\gamma \rho_0 p_0}\, u^C_{rms}}{p_{rms}} \approx 1. \tag{3.8}$$

As shown in table 2, $\sqrt{\gamma \rho_0 p_0}\, u^C_{rms}/p_{rms}$ is close to 1 in the numerical simulations, implying that the compressible velocity component is dominated by acoustic waves.

4. Spectra of velocity and thermodynamic variables

The compensated spectrum $E^u(k)\epsilon^{-2/3}k^{5/3}$ of the velocity field is plotted in figure 1(*a*). The velocity spectrum $E^u(k)$ satisfies $\int_0^\infty E^u(k)\,\mathrm{d}k = \langle \boldsymbol{u}^2\rangle/2$. An inertial range of the velocity spectrum is observed, namely, $E^u(k)k^{5/3}\epsilon^{-2/3}k^{5/3} \approx C_K$, where the Kolmogorov constant C_K is approximately 1.6, which is similar to the previous results of the velocity spectrum in compressible isotropic turbulence (Wang *et al.* 2012; Jagannathan & Donzis 2016; Wang *et al.* 2017). The compensated spectrum $E^{u,C}(k)\epsilon^{-2/3}k^{5/3}$ of the compressible velocity component is depicted in figure 1(*b*). The spectrum of compressible velocity $E^{u,C}(k)$ satisfies $\int_0^\infty E^{u,C}(k)\,\mathrm{d}k = \langle (u^C)^2/2\rangle$. It is found that $E^{u,C}(k)k^{5/3}\epsilon^{-2/3} \approx 0.2$ and 0.1 respectively for $M_t = 0.2$ and 0.6 for a short range of wavenumbers $0.015 \leqslant k\eta \leqslant 0.05$. The $k^{-5/3}$ scaling of compressible velocity spectrum $E^{u,C}(k)$ was also observed at $M_t \geqslant 0.6$ in solenoidally forced stationary compressible isotropic turbulence without any heat source, where the acoustic mode dominates the dynamics of the compressible velocity component (Wang *et al.* 2017). In the previous study, the k^{-3} scaling of the compressible velocity spectrum was identified in the range of wavenumber where the pseudosound mode is predominant over the acoustic mode at $M_t = 0.2$ (Wang *et al.* 2017). In contrast, we observe the $k^{-5/3}$ scaling of the compressible velocity spectrum at $M_t = 0.2$ in this study. The different scaling behaviour of the compressible velocity spectrum can be attributed to the fact that the heat source can generate acoustic waves which dominate the dynamics of the compressible velocity component at $M_t = 0.2$.

The normalized density fluctuation spectrum $E^\rho(k)/(\rho_{rms})^2$ and normalized pressure fluctuation spectrum $E^p(k)/(p_{rms})^2$ are plotted in figure 2, where $E^\rho(k)$ and $E^p(k)$ satisfy $\int_0^\infty E^\rho(k)\,\mathrm{d}k = (\rho_{rms})^2$ and $\int_0^\infty E^p(k)\,\mathrm{d}k = (p_{rms})^2$, respectively. It is shown that the spectra of density and pressure exhibit the $k^{-5/3}$ scaling for both turbulent Mach numbers $M_t = 0.2$ and 0.6. The effect of the turbulent Mach number on the normalized spectra is weak. The $k^{-5/3}$ scaling of spectra of density and pressure was also identified at $M_t \geqslant 0.5$ in solenoidally forced stationary compressible isotropic turbulence without any heat source (Wang *et al.* 2017). In the previous study, the $k^{-7/3}$ scaling of the spectra of density and pressure was identified at $M_t = 0.2$ where the solenoidal component of pressure is predominant over the compressible pressure component (Wang *et al.* 2017). In contrast, the spectra of density and pressure exhibit the $k^{-5/3}$ at $M_t = 0.2$ in this study, which can be attributed to the acoustic waves generated by the heat source.

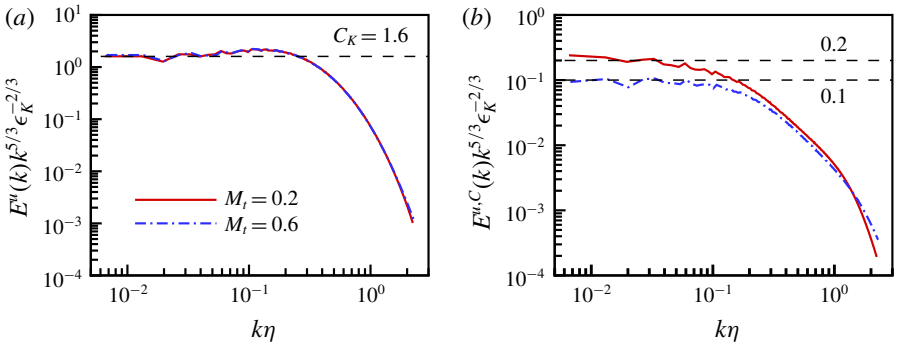

FIGURE 1. (Colour online) Compensated spectra of velocity and compressible velocity component at $M_t = 0.2,\ 0.6$: (*a*) $E^u(k)k^{5/3}\epsilon^{-2/3}$; (*b*) $E^{u,C}(k)k^{5/3}\epsilon^{-2/3}$.

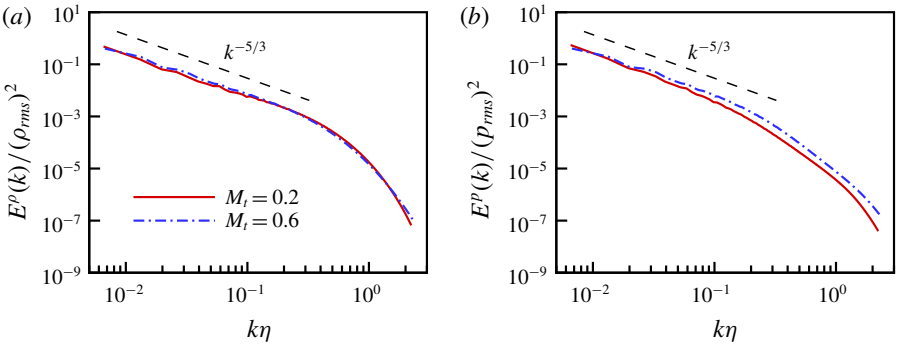

FIGURE 2. (Colour online) Normalized spectra of density and pressure at $M_t = 0.2,\ 0.6$: (*a*) $E^\rho(k)/(\rho_{rms})^2$; (*b*) $E^p(k)/(p_{rms})^2$.

The strong acoustic equilibrium can be expressed as (Sarkar *et al.* 1991; Sagaut & Cambon 2008; Jagannathan & Donzis 2016; Wang *et al.* 2017; Chen *et al.* 2018; Wang *et al.* 2018*b*)

$$E^p(k) \approx 2\rho_0^2 c_0^2 E^{u,C}(k). \tag{4.1}$$

Equation (4.1) is equivalent to

$$E^p(k)/(p_{rms})^2 \approx 2E^{u,C}(k)/(u^C_{rms})^2. \tag{4.2}$$

Both the normalized pressure fluctuation spectrum $E^p(k)/(p_{rms})^2$ and the normalized spectrum of the compressible velocity component $2E^{u,C}(k)/(u^C_{rms})^2$ are depicted in figure 3. It is found that $E^p(k)/(p_{rms})^2$ is very close to $2E^{u,C}(k)/(u^C_{rms})^2$ at $M_t = 0.2$, 0.6 in the numerical simulations. The observation confirms that the dynamics of the compressible velocity and the pressure is dominated by acoustic waves.

It is well known that the Kovasznay decomposition can be used to decompose a small-amplitude motion of a compressible fluid into vorticity, acoustic and entropic modes under the assumption that the effects of compressibility are very small (Kovasznay 1953; Sagaut & Cambon 2008). In compressible turbulent flow, the acoustic modes (or isentropic modes) of thermodynamic variables can be calculated

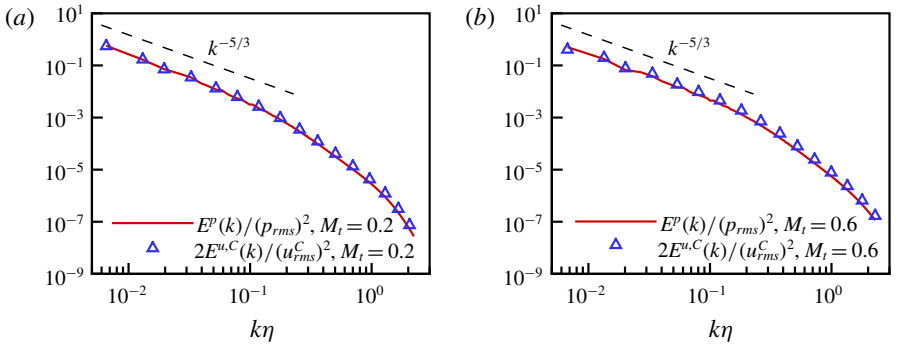

FIGURE 3. (Colour online) Normalized spectra of pressure and compressible velocity component at $M_t = 0.2,\ 0.6$: (*a*) $M_t = 0.2$; (*b*) $M_t = 0.6$.

by (Chassaing *et al.* 2002; Gauthier 2017)

$$p^I = p - p_0, \tag{4.3}$$

$$\rho^I = \frac{\rho_0 p^I}{\gamma p_0}, \tag{4.4}$$

$$T^I = \frac{(\gamma - 1) T_0 p^I}{\gamma p_0}, \tag{4.5}$$

and the entropic modes can be given by (Chassaing *et al.* 2002; Gauthier 2017)

$$p^E = 0, \tag{4.6}$$

$$\rho^E = \rho - \rho_0 - \rho^I, \tag{4.7}$$

$$T^E = T - T_0 - T^I. \tag{4.8}$$

It was shown that the spectra of the entropic modes of density, pressure and temperature are much smaller than those of the isentropic modes of density, pressure and temperature at $M_t \leqslant 1$ in solenoidally forced stationary compressible isotropic turbulence without any heat source (Wang *et al.* 2017), and at $M_t \leqslant 0.65$ in stationary compressible isotropic turbulence driven by both solenoidal and compressible forces without any heat source (Wang *et al.* 2018*b*).

The normalized spectra of the isentropic and entropic modes of density $E^{\rho,I}(k)/(\rho_{rms})^2$ and $E^{\rho,E}(k)/(\rho_{rms})^2$ are shown in figure 4, where the spectra $E^{\rho,I}(k)$ and $E^{\rho,E}(k)$ satisfy $\int_0^\infty E^{\rho,I}(k)\,\mathrm{d}k = \langle(\rho^I)^2\rangle$ and $\int_0^\infty E^{\rho,E}(k)\,\mathrm{d}k = \langle(\rho^E)^2\rangle$, respectively. It is found that the spectrum of the entropic mode of density is comparable to that of the isentropic mode of density at $M_t = 0.6$. Moreover, the spectrum of the entropic mode of density is much larger than that of the isentropic mode of density at $M_t = 0.2$. The observations are different from those in compressible isotropic turbulence without any heat source (Wang *et al.* 2017, 2018*b*), which can be attributed to the generation of the entropic modes of thermodynamic variables by the heat source.

Figure 5 shows that both the temperature fluctuation spectrum $E^T(k)$ and the entropy fluctuation spectrum $E^s(k)$ exhibit the $k^{-5/3}$ scaling behaviour in an inertial range of $0.02 \leqslant k\eta \leqslant 0.08$ at $M_t = 0.2,\ 0.6$, where η is the Kolmogorov length scale. Moreover, the compensated fluctuation spectra of temperature and entropy are nearly constant in

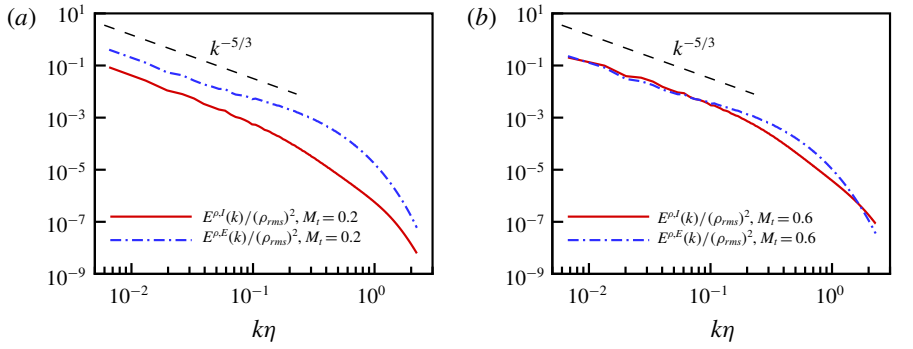

FIGURE 4. (Colour online) Normalized spectra of the entropic and isentropic modes of density at $M_t = 0.2,\ 0.6$: (*a*) $M_t = 0.2$; (*b*) $M_t = 0.6$.

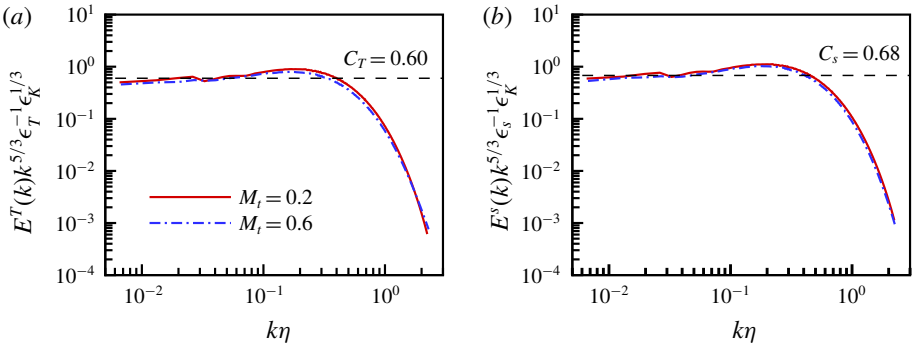

FIGURE 5. (Colour online) Compensated spectra of temperature and entropy fluctuations at $M_t = 0.2,\ 0.6$: (*a*) $E^T(k)k^{5/3}\epsilon_T^{-1}\epsilon_K^{1/3}$; (*b*) $E^s(k)k^{5/3}\epsilon_s^{-1}\epsilon_K^{1/3}$.

the inertial range, i.e. $E^T(k)k^{5/3}\epsilon_T^{-1}\epsilon_K^{1/3} \approx C_T$ and $E^s(k)k^{5/3}\epsilon_s^{-1}\epsilon_K^{1/3} \approx C_s$. The constants $C_T = 0.60$ and $C_s = 0.68$ are close to the typical Obukhov–Corrsin constant 0.7 of a passive scalar spectrum (Obukhov 1949; Corrsin 1951; Sreenivasan 1996; Yeung, Donzis & Sreenivasan 2005; Gotoh & Watanabe 2015). This observation indicates that the fluctuation spectra of both temperature and entropy can be well described by the Obukhov–Corrsin theory of a passive scalar (Obukhov 1949; Corrsin 1951).

The compensated spectra of the isentropic and entropic modes of temperature $E^{T,I}(k)k^{5/3}\epsilon_T^{-1}\epsilon_K^{1/3}$ and $E^{T,E}(k)k^{5/3}\epsilon_T^{-1}\epsilon_K^{1/3}$ are plotted in figure 6. It is shown that the spectrum of the entropic mode of temperature is much larger than that of the isentropic mode of temperature at $M_t = 0.2,\ 0.6$. The spectrum of the isentropic mode of temperature decreases rapidly with the decrease of turbulent Mach number, while the spectrum of the entropic mode of temperature increases slightly with the decrease of turbulent Mach number. Moreover, the compensated fluctuation spectrum of the entropic mode of temperature is nearly constant in the inertial range, i.e. $E^{T,E}(k)k^{5/3}\epsilon_T^{-1}\epsilon_K^{1/3} \approx 0.6$ and 0.5 for turbulent Mach numbers $M_t = 0.2$ and 0.6, respectively.

The $k^{-5/3}$ scaling behaviours of the spectra of the compressible velocity component, density, pressure, temperature and entropy are observed in our numerical simulations. To further confirm these scaling behaviours, we perform numerical simulations

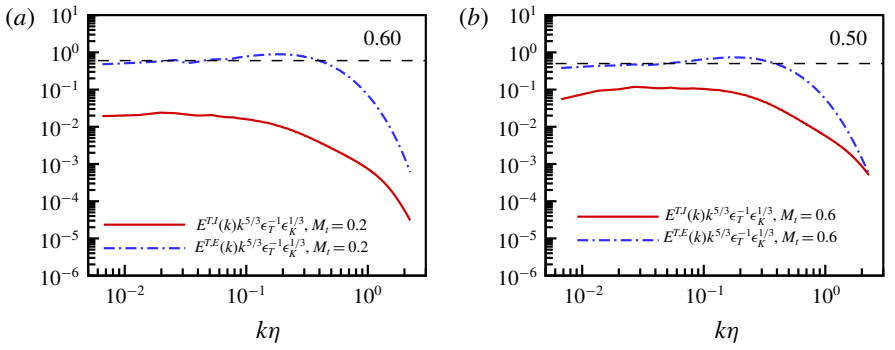

FIGURE 6. (Colour online) Compensated spectra of the isentropic and entropic modes of temperature at $M_t = 0.2,\ 0.6$: (*a*) $M_t = 0.2$; (*b*) $M_t = 0.6$.

Resolution	M_t	u'	u^S_{rms}	u^C_{rms}
512^3	0.20	2.32	2.17	0.81
512^3	0.61	2.32	2.25	0.54

TABLE 3. Statistics of velocity and its two components in hyperviscosity simulations.

M_t	p_0	T_0	s_0	p_{rms}/p_0	ρ_{rms}/ρ_0	T_{rms}/T_0	s_{rms}
0.20	92.2	1.03	0.03	0.10	0.17	0.16	0.22
0.61	10.2	1.01	0.01	0.22	0.21	0.16	0.20

TABLE 4. Statistics of thermodynamic variables in hyperviscosity simulations.

of Euler equations with an eighth-order hyperviscosity (Wang *et al.* 2010, 2013), at the same turbulent Mach numbers $M_t = 0.2,\ 0.6$ and at 512^3 grid resolution. Statistics of velocity, solenoidal velocity component, compressible velocity component and thermodynamic variables in hyperviscosity simulations are summarized in tables 3–4. The r.m.s. values of velocity, solenoidal velocity component, compressible velocity component and thermodynamic variables are close to those in the numerical simulations of the Navier–Stokes equations as shown in tables 1–2.

Normalized spectra of the velocity, compressible velocity component, density, pressure, temperature and entropy in the hyperviscosity simulations are plotted in figures 7–9. The spectra exhibit the $k^{-5/3}$ scaling more clearly for a range of $0.02 \leqslant k\Delta \leqslant 0.2$, as compared to the situation of the numerical simulations of the Navier–Stokes equations. Provided that the inertial-range statistics are independent of the dissipation mechanism (Benzi *et al.* 2008), the spectra of the velocity and thermodynamic variables will exhibit clearer $k^{-5/3}$ scaling behaviours at higher Reynolds numbers in compressible isotropic turbulence with a heat source by the numerical simulations of the Navier–Stokes equations.

5. Inter-scale transfer of temperature and entropy fluctuations

We apply the Favre filtering approach (Aluie 2011, 2013; Eyink & Drivas 2018; Wang *et al.* 2018*a*) to study the inter-scale transfer of temperature and entropy.

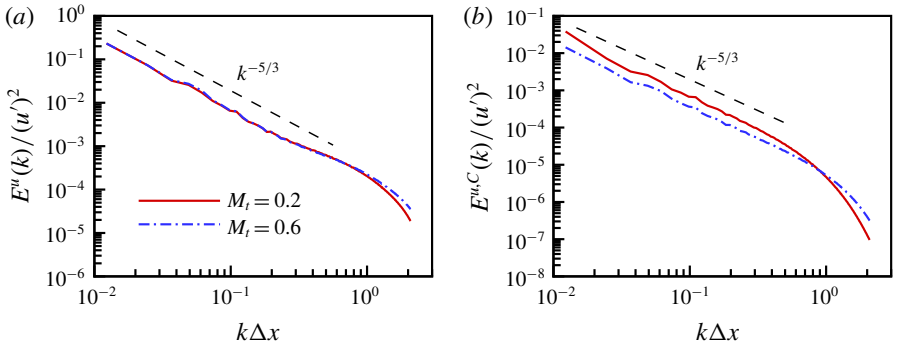

FIGURE 7. (Colour online) Normalized spectra of velocity and compressible velocity component at $M_t = 0.2$, 0.6 in hyperviscosity simulations: (*a*) $E^u(k)/(u')^2$; (*b*) $E^{u,C}(k)/(u')^2$.

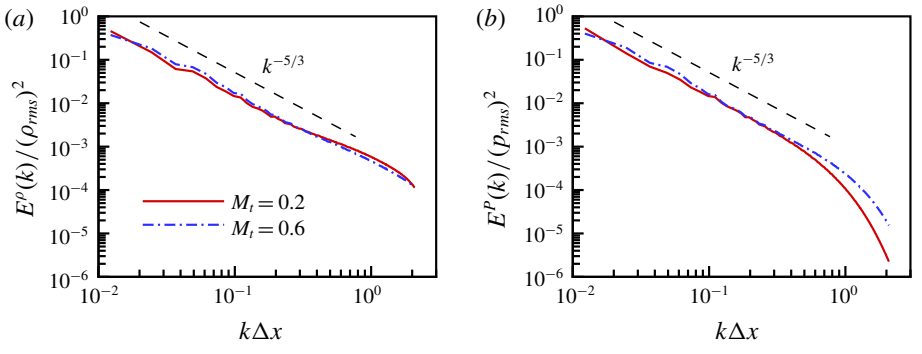

FIGURE 8. (Colour online) Normalized spectra of density and pressure at $M_t = 0.2$, 0.6 in hyperviscosity simulations: (*a*) $E^\rho(k)/(\rho_{rms})^2$; (*b*) $E^p(k)/(p_{rms})^2$.

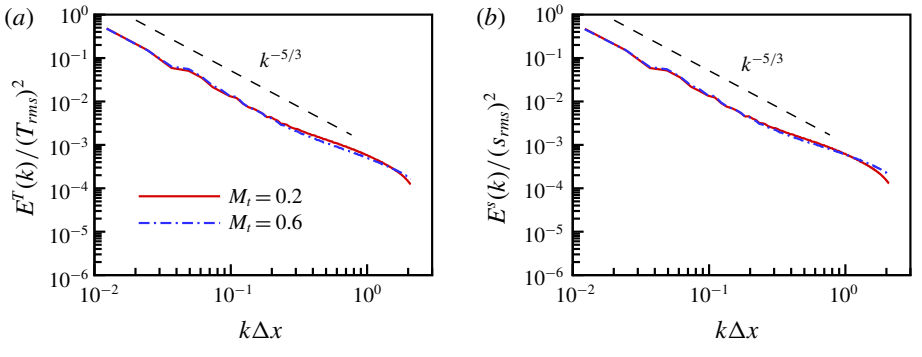

FIGURE 9. (Colour online) Normalized spectra of temperature and entropy at $M_t = 0.2$, 0.6 in hyperviscosity simulations: (*a*) $E^T(k)/(T_{rms})^2$; (*b*) $E^s(k)/(s_{rms})^2$.

A classically filtered field $\bar{f}$ is defined as $\bar{f}(\boldsymbol{x}) = \int \mathrm{d}^3\boldsymbol{r} G_l(\boldsymbol{r}) f(\boldsymbol{x}+\boldsymbol{r})$. Here, $G_l(\boldsymbol{r}) = l^{-3}G(\boldsymbol{r}/l)$ is the filter function, $G(\boldsymbol{r})$ is a normalized window function and l is the filter width. The Favre filtered field $\widetilde{f}$ is defined as $\widetilde{f} = \overline{\rho f}/\overline{\rho}$. The equation for the

r.m.s. value of the filtered temperature reads:

$$\frac{\partial}{\partial t}\langle \widetilde{T}_1^2\rangle = -\langle \Phi_l^T + \Pi_l^T + D_l^T + F_l^T\rangle, \tag{5.1}$$

where, Φ_l^T is the dilatation term, Π_l^T is the subgrid-scale (SGS) term, D_l^T represents the effect of thermal diffusion and viscous dissipation and F_l^T represents the effect of large-scale forcing. Here, $\Phi_l^T = -(3-2\gamma)\widetilde{T}_1^2\theta_l + 2(\gamma-1)T_0\widetilde{T}_1\theta_l$, $\theta_l = \partial\widetilde{u}_j/\partial x_j$, $\Pi_l^T = \Pi_l^{T,1} + \Pi_l^{T,2}$, $D_l^T = -2\widetilde{T}_1(\widetilde{D_\kappa} + \widetilde{D_\mu})$ and $F_l^T = -2\widetilde{T}_1\widetilde{f_T}$. $\Pi_l^{T,1} = -2[\overline{\rho}(\widetilde{T_1 u_j} - \widetilde{T}_1\widetilde{u}_j)](\partial/\partial x_j)(\widetilde{T}_1/\overline{\rho})$, and $\Pi_l^{T,2} = 2(\gamma-1)\widetilde{T}_1(\widetilde{T_1\theta} - \widetilde{T}_1\theta_l)$. $\Pi_l^{T,1}$ and $\Pi_2^{T,2}$ represent the SGS fluxes induced by the correlation between temperature and velocity, and by the correlation between temperature and velocity divergence, respectively.

The equation for the r.m.s. value of filtered entropy can be written as:

$$\frac{\partial}{\partial t}\langle \widetilde{s}_1^2\rangle = -\langle \Phi_l^s + \Pi_l^s + D_l^s + F_l^s\rangle, \tag{5.2}$$

where, Φ_l^s is the dilatation term, Π_l^s is the subgrid-scale (SGS) term, D_l^s represents the effect of thermal diffusion and viscous dissipation and F_l^s represents the effect of large-scale forcing. Here, $\Phi_l^s = -\widetilde{s}_1^2\theta_l$, $\Pi_l^s = -2[\overline{\rho}(\widetilde{s_1 u_j} - \widetilde{s}_1\widetilde{u}_j)](\partial/\partial x_j)(\widetilde{s}_1/\overline{\rho})$, $D_l^s = -2\widetilde{s}_1(\widetilde{D_\kappa/T} + \widetilde{D_\mu/T})$, and $F_l^s = -2\widetilde{s}_1\widetilde{f_T/T}$.

We plot spatial average values of $\langle \Phi_l^T + \Pi_l^T + D_l^T\rangle/\epsilon_T$, $\langle \Phi_l^T\rangle/\epsilon_T$, $\langle \Pi_l^T\rangle/\epsilon_T$ and $\langle D_l^T\rangle/\epsilon_T$ at $M_t = 0.2$, 0.6 in figure 10. We also plot spatial average values of $\langle \Phi_l^s + \Pi_l^s + D_l^s\rangle/\epsilon_s$, $\langle \Phi_l^s\rangle/\epsilon_s$, $\langle \Pi_l^s\rangle/\epsilon_s$ and $\langle D_l^s\rangle/\epsilon_s$ at $M_t = 0.2$, 0.6 in figure 11. The filter width l has been normalized by the Kolmogorov length scale η. It is shown that $\langle \Phi_l^T + \Pi_l^T + D_l^T\rangle/\epsilon_T \approx 1$ and $\langle \Phi_l^s + \Pi_l^s + D_l^s\rangle/\epsilon_s \approx 1$ for $l/\eta \leqslant 120$, indicating that the effects of large-scale forcing on inter-scale transfer processes of temperature and entropy fluctuations are localized to the large scales. $\langle \Pi_l^T\rangle/\epsilon_T$ and $\langle \Pi_l^s\rangle/\epsilon_s$ are nearly constant and are close to 1.0, over an inertial range $30 \leqslant l/\eta \leqslant 120$. Moreover, $\langle \Pi_l^T\rangle/\epsilon_T$ and $\langle \Pi_l^s\rangle/\epsilon_s$ decrease slightly with the increase of turbulent Mach number. It is found that terms $\langle \Phi_l^T\rangle$, $\langle D_l^T\rangle$, $\langle F_l^T\rangle$, $\langle \Phi_l^s\rangle$, $\langle D_l^s\rangle$ and $\langle F_l^s\rangle$ are small in the inertial range. It is also found that $\langle \Pi_l^{T,1}\rangle/\epsilon_T$ is much larger than $\langle \Pi_l^{T,2}\rangle/\epsilon_T$. These observations indicate the existence of direct cascades of temperature and entropy fluctuations from large scales to small scales through the inertial range.

The SGS fluxes of temperature due to the solenoidal and compressible modes of the velocity are, respectively,

$$\Pi_l^{T,S} = -2\left[\overline{\rho}(\widetilde{T_1 u_j^S} - \widetilde{T}_1\widetilde{u}_j^S)\right]\frac{\partial}{\partial x_j}\left(\frac{\widetilde{T}_1}{\overline{\rho}}\right), \tag{5.3}$$

and,

$$\Pi_l^{T,C} = -2\left[\overline{\rho}(\widetilde{T_1 u_j^C} - \widetilde{T}_1\widetilde{u}_j^C)\right]\frac{\partial}{\partial x_j}\left(\frac{\widetilde{T}_1}{\overline{\rho}}\right) + \Pi_l^{T,2}. \tag{5.4}$$

Similarly, the SGS fluxes of entropy due to the solenoidal and compressible modes of the velocity are, respectively,

$$\Pi_l^{s,S} = -2\left[\overline{\rho}(\widetilde{s_1 u_j^S} - \widetilde{s}_1\widetilde{u}_j^S)\right]\frac{\partial}{\partial x_j}\left(\frac{\widetilde{s}_1}{\overline{\rho}}\right), \tag{5.5}$$

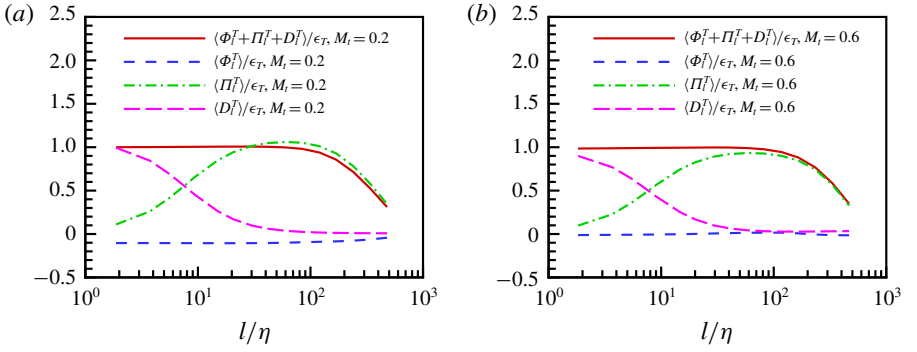

FIGURE 10. (Colour online) Average values of $\langle \Phi_l^T + \Pi_l^T + D_l^T\rangle/\epsilon_T$, $\langle \Phi_l^T\rangle/\epsilon_T$, $\langle \Pi_l^T\rangle/\epsilon_T$ and $\langle D_l^T\rangle/\epsilon_T$ at $M_t = 0.2,\ 0.6$: (*a*) $M_t = 0.2$; (*b*) $M_t = 0.6$.

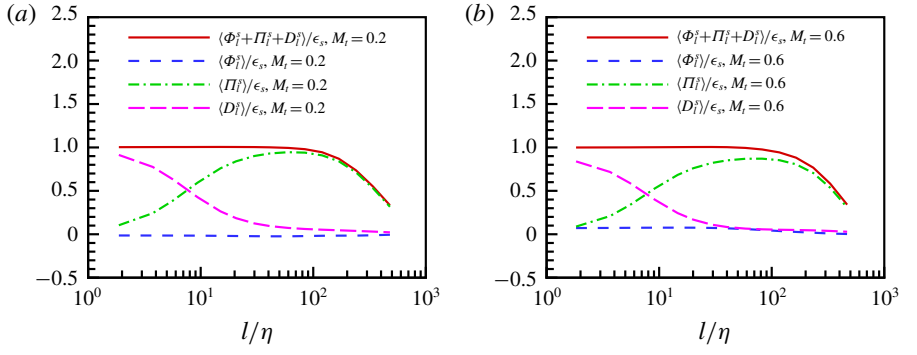

FIGURE 11. (Colour online) Average values of $\langle \Phi_l^s + \Pi_l^s + D_l^s\rangle/\epsilon_s$, $\langle \Phi_l^s\rangle/\epsilon_s$, $\langle \Pi_l^s\rangle/\epsilon_s$ and $\langle D_l^s\rangle/\epsilon_s$ at $M_t = 0.2,\ 0.6$: (*a*) $M_t = 0.2$; (*b*) $M_t = 0.6$.

and,

$$\Pi_l^{s,C} = -2\left[\overline{\rho}(\widetilde{s_1 u_j^C} - \widetilde{s}_1\widetilde{u}_j^C)\right]\frac{\partial}{\partial x_j}\left(\frac{\widetilde{s}_1}{\overline{\rho}}\right). \tag{5.6}$$

Here, $\widetilde{\boldsymbol{u}}^S$ and $\widetilde{\boldsymbol{u}}^C$ are the solenoidal and compressible components of the filtered velocity field $\widetilde{\boldsymbol{u}}$, respectively.

We plot spatial average values of SGS fluxes of temperature and entropy due to the solenoidal and compressible modes of velocity at $M_t = 0.2,\ 0.6$ in figure 12. It is found that $\langle \Pi_l^{T,S}\rangle/\epsilon_T \approx 0$ and $\langle \Pi_l^{s,C}\rangle/\epsilon_s \approx 0$, namely, $\langle \Pi_l^{T,C}\rangle/\epsilon_T \approx \langle \Pi_l^T\rangle/\epsilon_T$ and $\langle \Pi_l^{s,S}\rangle/\epsilon_s \approx \langle \Pi_l^s\rangle/\epsilon_s$. Thus, the average SGS flux of temperature is dominated by the compressible mode of the velocity field, indicating that the theory of a passive scalar in incompressible turbulence, which was often used for the temperature field in compressible turbulence, is not suitable to describe the inter-scale transfer of temperature in compressible turbulence. The average SGS flux of entropy is dominated by the solenoidal mode of the velocity field, which is similar to that of a passive scalar in incompressible turbulence.

The probability density functions (PDFs) of the SGS fluxes of temperature and entropy for $l/\eta = 16,\ 32,\ 64$ at $M_t = 0.2,\ 0.6$ are depicted in figure 13. It is shown that the PDFs of SGS fluxes exhibit a skewness toward the positive side, suggesting

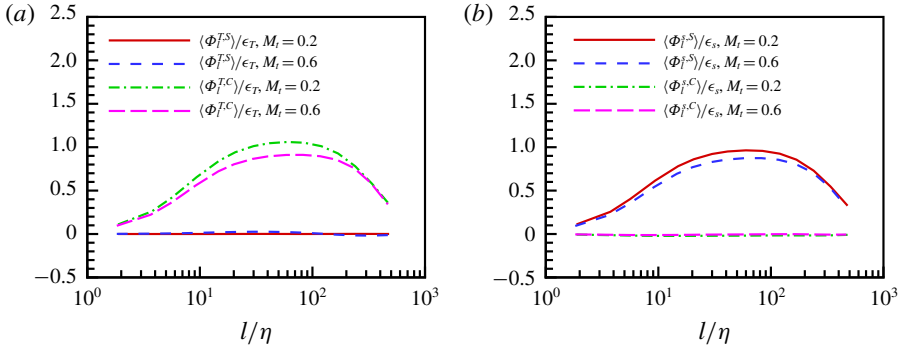

FIGURE 12. (Colour online) Average values of SGS fluxes of temperature and entropy due to the solenoidal and compressible modes of velocity at $M_t = 0.2$, 0.6: (*a*) $\langle \Pi_l^{T,S}\rangle/\epsilon_T$ and $\langle \Pi_l^{T,C}\rangle/\epsilon_T$; (*b*) $\langle \Pi_l^{s,S}\rangle/\epsilon_s$ and $\langle \Pi_l^{s,C}\rangle/\epsilon_s$.

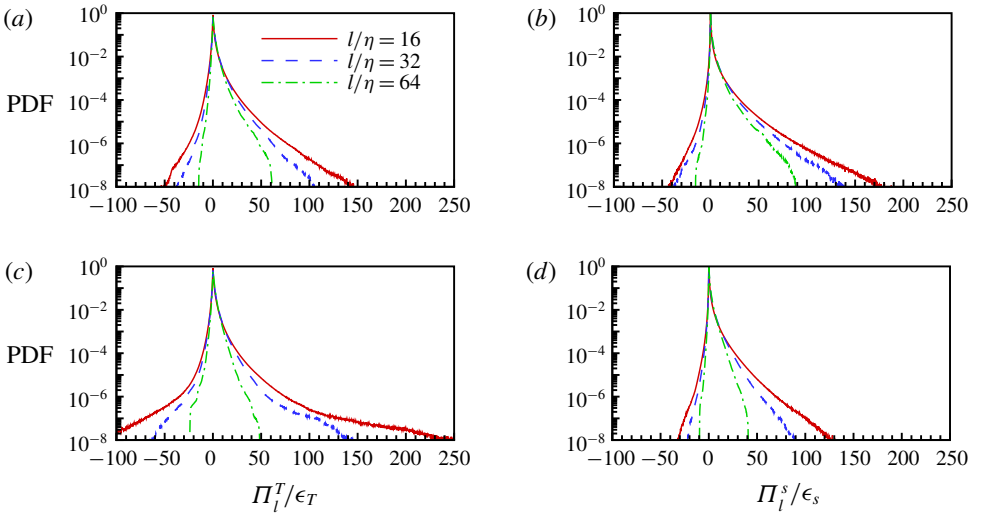

FIGURE 13. (Colour online) PDFs of SGS fluxes of temperature and entropy for $l/\eta = 16$, 32, 64 at $M_t = 0.2$, 0.6: (*a*) PDFs of Π_l^T/ϵ_T at $M_t = 0.2$; (*b*) PDFs of Π_l^s/ϵ_s at $M_t = 0.2$; (*c*) PDFs of Π_l^T/ϵ_T at $M_t = 0.6$; (*d*) PDFs of Π_l^s/ϵ_s at $M_t = 0.6$.

that the SGS fluxes of temperature and entropy have a tendency to direct from large scales to small scales. The tails of PDFs become longer as the filter width l decreases. The tails of PDFs of Π_l^T/ϵ_T are slightly shorter than those of Π_l^s/ϵ_s at $M_t = 0.2$. As turbulent Mach number increases to $M_t = 0.6$, the tails of PDFs of Π_l^T/ϵ_T become longer while the tails of PDFs of Π_l^s/ϵ_s become shorter. This observation indicates that the extremely high magnitude of the SGS temperature flux is enhanced and the extremely high magnitude of the SGS entropy flux is suppressed with the increase of turbulent Mach number. The tails of the PDFs of Π_l^T/ϵ_T are significantly longer than those of Π_l^s/ϵ_s at $M_t = 0.6$.

Figure 14 shows the PDFs of the SGS fluxes of temperature and entropy due to two components of the velocity for $l/\eta = 16$ at $M_t = 0.2$, 0.6. It is found that the PDF of $\Pi_l^{T,C}/\epsilon_T$ is similar to that of Π_l^T/ϵ_T, which is consistent with the previous

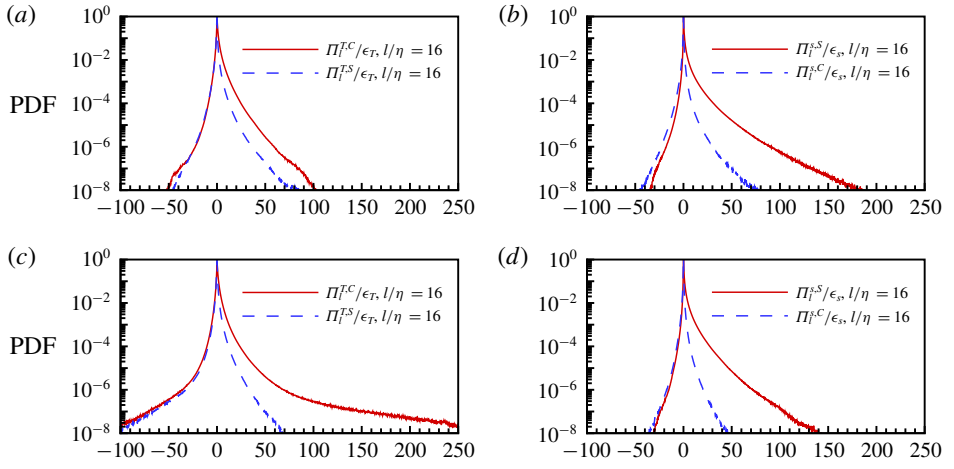

FIGURE 14. (Colour online) PDFs of SGS fluxes of temperature and entropy due to two components of the velocity for $l/\eta = 16$ at $M_t = 0.2,\ 0.6$: (*a*) PDFs of $\Pi_l^{T,C}/\epsilon_T$ and $\Pi_l^{T,S}/\epsilon_T$ at $M_t = 0.2$; (*b*) PDFs of $\Pi_l^{s,S}/\epsilon_s$ and $\Pi_l^{s,C}/\epsilon_s$ at $M_t = 0.2$; (*c*) PDFs of $\Pi_l^{T,C}/\epsilon_T$ and $\Pi_l^{T,S}/\epsilon_T$ at $M_t = 0.6$; (*d*) PDFs of $\Pi_l^{s,S}/\epsilon_s$ and $\Pi_l^{s,C}/\epsilon_s$ at $M_t = 0.6$.

observation that the average SGS flux of temperature is dominated by the compressible velocity component. The right tail of the PDF of $\Pi_l^{T,S}/\epsilon_T$ is significantly shorter than that of $\Pi_l^{T,C}/\epsilon_T$, implying that the contribution of the solenoidal velocity component to the average SGS temperature flux is significantly smaller than that of the compressible velocity component. Similarly, the PDF of $\Pi_l^{s,S}/\epsilon_s$ is similar to that of Π_l^s/ϵ_s, giving rise to the fact that the average SGS flux of entropy is dominated by the solenoidal velocity component. The right tail of the PDF of $\Pi_l^{s,C}/\epsilon_T$ is much shorter than that of $\Pi_l^{s,S}/\epsilon_T$, suggesting that the contribution of the compressible velocity component to the average SGS entropy flux is much smaller than that of the solenoidal velocity component.

Now we define the following geometrical variables for the SGS fluxes of temperature and entropy: $\phi_l^T = \boldsymbol{Q}^T \cdot \boldsymbol{G}^T/(|\boldsymbol{Q}^T|\,|\boldsymbol{G}^T|)$, and $\phi_l^s = \boldsymbol{Q}^s \cdot \boldsymbol{G}^s/(|\boldsymbol{Q}^s|\,|\boldsymbol{G}^s|)$, where $Q_j^T = \overline{\rho}(\widetilde{T_1 u_j} - \widetilde{T}_1\widetilde{u}_j)$, $G_j^T = (\partial/\partial x_j)(\widetilde{T}_1/\overline{\rho})$, $Q_j^s = \overline{\rho}(\widetilde{s_1 u_j} - \widetilde{s}_1\widetilde{u}_j)$ and $G_j^s = (\partial/\partial x_j)(\widetilde{s}_1/\overline{\rho})$. Similarly, we can define the geometrical variables for SGS fluxes of temperature and entropy due to two components of the velocity as follows: $\phi_l^{T,X} = \boldsymbol{Q}^{T,X} \cdot \boldsymbol{G}^T/(|\boldsymbol{Q}^{T,X}|\,|\boldsymbol{G}^T|)$, and $\phi_l^{s,X} = \boldsymbol{Q}^{s,X} \cdot \boldsymbol{G}^s/(|\boldsymbol{Q}^{s,X}|\,|\boldsymbol{G}^s|)$, where $Q_j^{T,X} = \overline{\rho}(\widetilde{T_1 u_j^X} - \widetilde{T}_1\widetilde{u}_j^X)$, $Q_j^{s,X} = \overline{\rho}(\widetilde{s_1 u_j^X} - \widetilde{s}_1\widetilde{u}_j^X)$ and $X = S,\ C$. We plot the PDFs of ϕ_l^T, $\phi_l^{T,S}$, $\phi_l^{T,C}$, ϕ_l^s, $\phi_l^{s,S}$ and $\phi_l^{s,C}$ at $M_t = 0.2,\ 0.6$ in figure 15. Both geometrical variables ϕ_l^T and ϕ_l^s have a tendency to be negative, in agreement with the overall direct cascade of temperature and entropy from large scales to small scales. It is found that the geometrical variable $\phi_l^{T,C}$ has a tendency to be -1, while the PDF of geometrical variable $\phi_l^{T,S}$ is nearly symmetrical with respect to $\phi_l^{T,S} = 0$. This observation partly explains why the cascade of temperature is dominated by the compressible mode of the velocity field. In contrast, the PDF of the geometrical variable $\phi_l^{s,C}$ is nearly symmetrical with respect to $\phi_l^{s,C} = 0$, while the PDF of the geometrical variable $\phi_l^{s,S}$ is almost identical to that of ϕ_l^s. The observation is consistent with the fact that the cascade of entropy

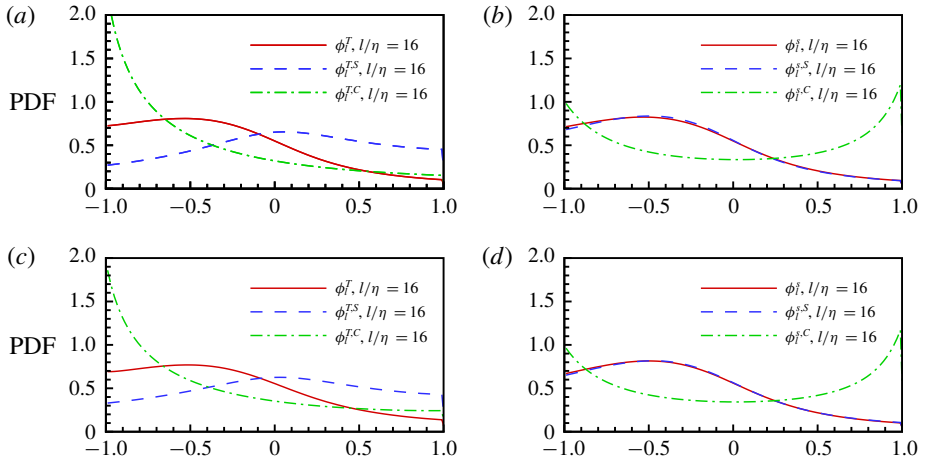

FIGURE 15. (Colour online) PDFs of geometrical variables for SGS fluxes of temperature and entropy, and their compressible and solenoidal components at $M_t = 0.2$, 0.6: (*a*) PDFs of ϕ_l^T, $\phi_l^{T,S}$ and $\phi_l^{T,C}$ at $M_t = 0.2$; (*b*) PDFs of ϕ_l^s, $\phi_l^{s,S}$ and $\phi_l^{s,C}$ at $M_t = 0.2$; (*c*) PDFs of ϕ_l^T, $\phi_l^{T,S}$ and $\phi_l^{T,C}$ at $M_t = 0.6$; (*d*) PDFs of ϕ_l^s, $\phi_l^{s,S}$ and $\phi_l^{s,C}$ at $M_t = 0.6$.

is dominated by the solenoidal mode of the velocity field. The effect of turbulent Mach number on the statistics of the geometrical variables is negligibly small.

To clarify the impact of local compression and expansion motions on the inter-scale transfer of temperature and entropy, we plot the average of SGS fluxes of temperature and entropy conditioned on the normalized filtered dilatation θ_l/θ_l' for $l/\eta = 16$ at $M_t = 0.2$, 0.6 in figure 16. Here, $\theta_l' = \sqrt{\langle\theta_l^2\rangle}$ is the r.m.s. value of the filtered dilatation. The fluctuations of the conditional average curves for $\theta_l/\theta_l' > 6$ are due to the lack of samples. It is shown that the conditional average SGS fluxes $\langle \Pi_l^T/\epsilon_T \,|\, \theta_l/\theta_l'\rangle$ and $\langle \Pi_l^s/\epsilon_s \,|\, \theta_l/\theta_l'\rangle$ increase with the increase of magnitude of the filtered dilatation in compression regions $\theta_l/\theta_l' < 0$, and decrease with the increase of magnitude of the filtered dilatation in expansion regions $\theta_l/\theta_l' > 0$. The observation indicates that compression motions enhance the direct SGS flux of temperature and entropy, while expansion motions suppress the direct SGS flux of temperature and entropy. Moreover, $\langle \Pi_l^T/\epsilon_T \,|\, \theta_l/\theta_l'\rangle$ becomes negative for $\theta_l/\theta_l' > 5$, giving rise to the reverse SGS flux of temperature from small scales to large scales in very strong expansion regions. It is worth noting that the magnitude of the conditional average SGS flux of the temperature in strong compression regions is much higher than that in strong expansion regions, demonstrating that the effect of compression motions on the inter-scale transfer of temperature is significantly larger than that of expansion motions. Moreover, the effect of compressibility on the inter-scale transfer of temperature is much stronger than on the inter-scale transfer of entropy, due to the explicit effect of velocity divergence term in the dynamical equation of temperature.

It is interesting to see that the conditional average $\langle \Pi_l^{T,S}/\epsilon_T \,|\, \theta_l/\theta_l'\rangle$ decreases with the increase of magnitude of the filtered dilatation in compression regions, and increases with the increase of magnitude of the filtered dilatation in expansion regions. The local compressibility effect on the SGS temperature flux due to the solenoidal velocity component $\Pi_l^{T,S}$ is opposite to the local compressibility effect on the overall SGS temperature flux Π_l^T. It is shown that the conditional average of the

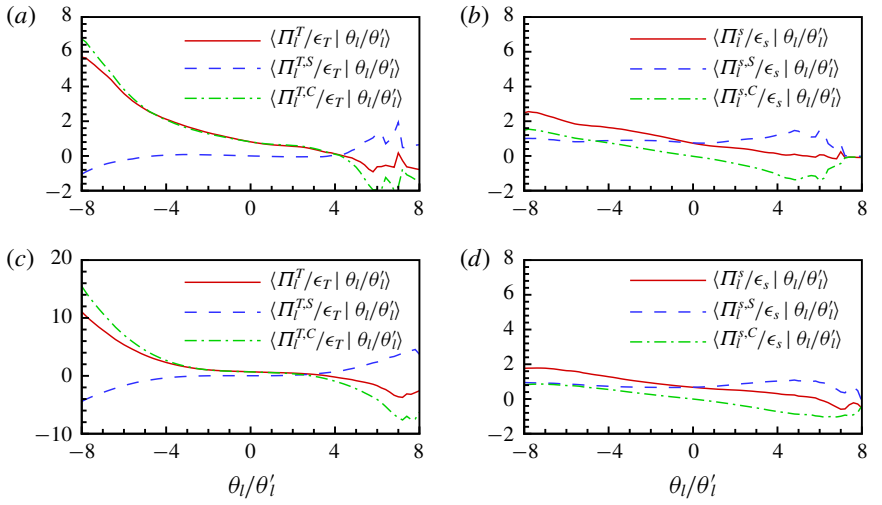

FIGURE 16. (Colour online) Conditional average SGS fluxes of temperature and entropy, and their compressible and solenoidal components for $l/\eta = 16$ at $M_t = 0.2$, 0.6: (*a*) $\langle \Pi_l^T/\epsilon_T \,|\, \theta_l/\theta_l' \rangle$, $\langle \Pi_l^{T,S}/\epsilon_T \,|\, \theta_l/\theta_l' \rangle$ and $\langle \Pi_l^{T,C}/\epsilon_T \,|\, \theta_l/\theta_l' \rangle$ at $M_t = 0.2$; (*b*) $\langle \Pi_l^{s}/\epsilon_s \,|\, \theta_l/\theta_l' \rangle$, $\langle \Pi_l^{s,S}/\epsilon_s \,|\, \theta_l/\theta_l' \rangle$ and $\langle \Pi_l^{s,C}/\epsilon_s \,|\, \theta_l/\theta_l' \rangle$ at $M_t = 0.2$; (*c*) $\langle \Pi_l^T/\epsilon_T \,|\, \theta_l/\theta_l' \rangle$, $\langle \Pi_l^{T,S}/\epsilon_T \,|\, \theta_l/\theta_l' \rangle$ and $\langle \Pi_l^{T,C}/\epsilon_T \,|\, \theta_l/\theta_l' \rangle$ at $M_t = 0.6$; (*d*) $\langle \Pi_l^{s}/\epsilon_s \,|\, \theta_l/\theta_l' \rangle$, $\langle \Pi_l^{s,S}/\epsilon_s \,|\, \theta_l/\theta_l' \rangle$ and $\langle \Pi_l^{s,C}/\epsilon_s \,|\, \theta_l/\theta_l' \rangle$ at $M_t = 0.6$.

SGS temperature flux due to the compressible velocity component $\Pi_l^{T,C}$ is similar to the conditional average of the overall SGS temperature flux Π_l^T. In addition, the magnitude of the conditional average of the SGS temperature flux due to the compressible velocity component is much larger than that of the SGS temperature flux due to the solenoidal velocity component in strong compression regions.

It is found that the conditional average $\langle \Pi_l^{s,S}/\epsilon_T \,|\, \theta_l/\theta_l' \rangle$ is close to 1.0 and is insensitive to the change of filtered dilatation, implying that the effect of local compressibility on the SGS entropy flux due to the solenoidal velocity component $\Pi_l^{s,S}$ is very weak. In compression regions, the conditional average $\langle \Pi_l^{s,C}/\epsilon_T \,|\, \theta_l/\theta_l' \rangle$ is positive, and increases with the increase of magnitude of the filtered dilatation. In expansion regions, the conditional average $\langle \Pi_l^{s,C}/\epsilon_T \,|\, \theta_l/\theta_l' \rangle$ is negative, and decreases with the increase of magnitude of filtered dilatation. The observation suggests that compression motions induce the direct SGS entropy flux due to the compressible velocity component $\Pi_l^{s,C}$ from large scales to small scales, which is balanced by the reverse SGS entropy flux due to the compressible velocity component $\Pi_l^{s,C}$ from small scales to large scales induced by expansion motions.

6. Discussion

Previous studies showed that the r.m.s. value of compressible velocity component is decreasing monotonically with the decrease of turbulent Mach number in solenoidally forced stationary compressible isotropic turbulence without any heat source (Jagannathan & Donzis 2016; Wang *et al.* 2017). Specifically, a M_t^4 scaling of the energy of compressible velocity component was identified at low turbulent Mach numbers where the pseudosound mode dominates the compressible dynamics

(Wang *et al.* 2017). However, the statistics of the compressible velocity component in compressible turbulence is not uniquely dependent on the turbulent Mach number. Another previous study showed that the ratios of r.m.s. values of the compressible velocity component to the solenoidal velocity component are insensitive to the change of turbulent Mach number, and are always larger than 0.64, at turbulent Mach numbers from 0.30 to 0.65 in the stationary compressible isotropic turbulence driven by both solenoidal and compressible forces (Wang *et al.* 2018*b*). We also found that the ratios of r.m.s. values of the compressible velocity component to the solenoidal velocity component can be larger than 0.64 at smaller turbulent Mach numbers $M_t \leqslant 0.1$ in the stationary compressible isotropic turbulence driven by both solenoidal and compressible forces. In this study, we observe that the r.m.s. value of the compressible velocity component is not decreasing with the decrease of turbulent Mach number in stationary compressible isotropic turbulence, which can be attributed to the acoustic waves generated by the heat source.

Bayly *et al.* (1992) predicted that entropy fluctuations obey the passive scalar transport equation in the inertial range, and the fluctuation spectrum of entropy is proportional to $k^{-5/3}$. Our numerical result on the entropy spectrum is consistent with the theoretical prediction made by Bayly *et al.* (1992). Pan & Scannapieco (2010, 2011) investigated the statistics and structures of a passive scalar in supersonic turbulence. They found that the compressible mode of velocity is less efficient in mixing the passive scalar than the solenoidal mode of velocity. They also showed that the degree of intermittency of the passive scalar increases only slightly as the flow changes from transonic to highly supersonic, which is due to the absence of shock-like discontinuities in the scalar field. Our numerical study shows that the inter-scale transfer of entropy is dominated by the solenoidal mode of the velocity field and is insensitive to the change of local compressibility, similar to the results of a passive scalar in compressible turbulence (Pan & Scannapieco 2010, 2011).

Eyink & Drivas (2018) recalled that the thermodynamic entropy per unit volume s is an analytic concave function of the internal energy per unit volume and the particle number per unit volume: $s = s(e_I, n)$, where e_I was defined as the internal energy per unit volume and n was defined as the particle number per unit volume. The large-scale or resolved entropy was defined by $\underline{s} = s(\overline{e_I}, \overline{n})$, and the small-scale or unresolved entropy was given by $\Delta s = \overline{s} - \underline{s}$, where $\overline{s} = \overline{s(e_I, n)}$. It was shown that $\Delta s \leqslant 0$, indicating that spatial coarse graining increases entropy. They showed an anomalous input of negative entropy by pressure work and a cascade of negative entropy to small scales with a rigorous detailed analysis provided in the companion paper (Drivas & Eyink 2018). Eyink & Drivas (2018) pointed out that the entropy in compressible turbulence is not at all a passive scalar due to their prediction of the inverse cascade of the entropy as a nonlinear function of e_I and n. It is worth noting that the definition of large-scale or resolved entropy is not unique. In this study, we have investigated numerically the inter-scale transfer of entropy fluctuations through the dynamical equation of the r.m.s. value of Favre filtered entropy $\widetilde{s}$, which differs from the large-scale entropy studied by Eyink & Drivas (2018). This difference and the specific flow forcing details could contribute to the different conclusions noted here. The numerical analysis method on the entropy transfer in this study can be applied directly to analyse the inter-scale transfer of other scalar variables, including temperature, passive scalar and pressure. We have also addressed the similarity and difference between the inter-scale transfer processes of temperature and entropy fluctuations.

7. Conclusions

In this paper, we have performed numerical simulations of stationary three-dimensional compressible isotropic turbulence with a heat source at turbulent Mach numbers $M_t = 0.2,\ 0.6$. We have shown that the spectra of velocity, compressible velocity component, density, pressure, temperature and entropy exhibit the $-5/3$ scaling in the inertial range. The strong acoustic equilibrium relation between spectra of the compressible velocity component and the pressure has been verified. Moreover, the spectra of the isentropic modes and entropic modes of thermodynamic variables have been studied by Kovasznay decomposition. The dynamics of the temperature field is dominated by the entropic mode due to the effect of heat source. The compensated fluctuation spectra of temperature and entropy are nearly constant in the inertial range, with the Obukhov–Corrsin constants close to that of a passive scalar spectrum.

We have applied a filtering method to investigate the inter-scale transfer of temperature and entropy. We have shown that both temperature and entropy fluctuations cascade from large scales to small scales. The cascade of temperature is dominated by the compressible mode of velocity field, while the cascade of entropy is dominated by the solenoidal mode of the velocity field. The geometrical properties of the SGS fluxes are reported to partly explain the difference between the cascades of temperature and entropy. The effect of local compressibility on the inter-scale transfer of temperature and entropy are studied through conditional averaging with respect to the filtered dilatation. It is shown that the effect of compressibility on the cascade of temperature is much stronger than on the cascade of entropy, due to the explicit effect of velocity divergence term in the dynamical equation of temperature.

Several issues require further investigation, including the connection between structures and the statistics of temperature and entropy, the interactions between thermodynamic variables and velocity field and the compressibility effects at higher turbulent Mach numbers.

Acknowledgements

This work was supported by the National Natural Science Foundation of China (NSFC grants nos. 11702127, 91752201, and 11672123), and by the Technology and Innovation Commission of Shenzhen Municipality (grant no. JCYJ20170412151759222). J.W. acknowledges support from the Young Elite Scientist Sponsorship Program by CAST (grant no. 2016QNRC001).

REFERENCES

ALUIE, H. 2011 Compressible turbulence: the cascade and its locality. *Phys. Rev. Lett.* **106**, 174502.

ALUIE, H. 2013 Scale decomposition in compressible turbulence. *Physica* D **247**, 54–65.

ALUIE, H., LI, S. & LI, H. 2012 Conservative cascade of kinetic energy in compressible turbulence. *Astrophys. J. Lett.* **751**, L29.

BALSARA, D. S. & SHU, C. W. 2000 Monotonicity preserving weighted essentially non-oscillatory schemes with increasingly high order of accuracy. *J. Comp. Phys.* **160**, 405–452.

BAYLY, B. J., LEVERMORE, C. D. & PASSOT, T. 1992 Density variations in weakly compressible flows. *Phys. Fluids* A **4**, 945–954.

BENZI, R., BIFERALE, L., FISHER, R. T., KADANOFF, L. P., LAMB, D. Q. & TOSCHI, F. 2008 Intermittency and universality in fully developed inviscid and weakly compressible turbulent flows. *Phys. Rev. Lett.* **100**, 234503.

CARDY, J., FALKOVICH, G. & GAWEDZKI, K. 2008 *Non-equilibrium Statistical Mechanics and Turbulence*. Cambridge University Press.

CHASSAING, P., ANTONIZ, R., ANSELMET, F., JOLY, L. & SARKAR, S. 2002 *Variable Density Fluid Turbulence, Fluid Mechanics and its Applications*, vol. 69. Kluwer.

CHEN, S. & CAO, N. 1997 Anomalous scaling and structure instability in three-dimensional passive scalar turbulence. *Phys. Rev. Lett.* **78**, 3459–3462.

CHEN, S., WANG, J., LI, H., WAN, M. & CHEN, S. Y. 2018 Spectra and Mach number scaling in compressible homogeneous shear turbulence. *Phys. Fluids* **30**, 065109.

CORRSIN, S. 1951 On the spectrum of isotropic temperature fluctuations in an isotropic turbulence. *J. Appl. Phys.* **22**, 469–473.

DONZIS, D. A. & MAQUI, A. F. 2016 Statistically steady states of forced isotropic turbulence in thermal equilibrium and non-equilibrium. *J. Fluid Mech.* **797**, 181–200.

DRIVAS, T. D. & EYINK, G. L. 2018 An Onsager singularity theorem for turbulent solutions of compressible Euler equations. *Commun. Math. Phys.* **359**, 733–763.

EYINK, G. L. & DRIVAS, T. D. 2018 Cascades and dissipative anomalies in compressible fluid turbulence. *Phys. Rev.* X **8**, 011022.

FALKOVICH, G., FOUXON, I. & OZ, Y. 2010 New relations for correlation functions in Navier–Stokes turbulence. *J. Fluid Mech.* **644**, 465–472.

FRISCH, U. 1995 *Turbulence: The Legacy of A. N. Kolmogorov*. Cambridge University Press.

GALTIER, S. & BANERJEE, S. 2011 Exact relation for correlation functions in compressible isothermal turbulence. *Phys. Rev. Lett.* **107**, 134501.

GAUTHIER, S. 2017 Compressible Rayleigh–Taylor turbulent mixing layer between Newtonian miscible fluids. *J. Fluid Mech.* **830**, 211–256.

GOTOH, T. & WATANABE, T. 2015 Power and nonpower laws of passive scalar moments convected by isotropic turbulence. *Phys. Rev. Lett.* **115**, 114502.

JAGANNATHAN, S. & DONZIS, D. A. 2016 Reynolds and Mach number scaling in solenoidally-forced compressible turbulence using high-resolution direct numerical simulations. *J. Fluid Mech.* **789**, 669–707.

KOVASZNAY, L. S. G. 1953 Turbulence in supersonic flow. *J. Aeronaut. Sci.* **20**, 657–674.

KRITSUK, A. G., WAGNER, R. & NORMAN, M. L. 2013 Energy cascade and scaling in supersonic isothermal turbulence. *J. Fluid Mech.* **729**, R1.

LELE, S. K. 1992 Compact finite difference schemes with spectral-like resolution. *J. Comput. Phys.* **103**, 16–42.

LIVESCU, D. & LI, Z. 2017 Subgrid-scale backscatter after the shock–turbulence interaction. *AIP Conf. Proc.* **1793**, 150009.

OBUKHOV, A. M. 1949 Structure of the temperature field in turbulent flows. *Isv. Akad. Nauk SSSR Geogr. Geofiz.* **13**, 58–69.

PAN, L. & SCANNAPIECO, E. 2010 Mixing in supersonic turbulence. *Astrophys. J.* **721**, 1765–1782.

PAN, L. & SCANNAPIECO, E. 2011 Passive scalar structures in supersonic turbulence. *Phys. Rev.* E **83**, 045302(R).

SAGAUT, P. & CAMBON, C. 2008 *Homogeneous Turbulence Dynamics*. Cambridge University Press.

SAMTANEY, R., PULLIN, D. I. & KOSOVIC, B. 2001 Direct numerical simulation of decaying compressible turbulence and shocklet statistics. *Phys. Fluids* **13**, 1415–1430.

SARKAR, S., ERLEBACHER, G., HUSSAINI, M. Y. & KREISS, H. O. 1991 The analysis and modelling of dilatational terms in compressible turbulence. *J. Fluid Mech.* **227**, 473–493.

SREENIVASAN, K. R. 1996 The passive scalar spectrum and the Obukhov–Corrsin constant. *Phys. Fluids* **8**, 189–196.

SUMAN, S. & GIRIMAJI, S. S. 2011 Dynamical model for velocity-gradient evolution in compressible turbulence. *J. Fluid Mech.* **683**, 289–319.

WAGNER, R., FALKOVICH, G., KRITSUK, A. G. & NORMAN, M. L. 2012 Flux correlations in supersonic isothermal turbulence. *J. Fluid Mech.* **713**, 482–490.

WANG, J., GOTOH, T. & WATANABE, T. 2017 Spectra and statistics in compressible isotropic turbulence. *Phys. Rev. Fluids* **2**, 013403.

WANG, J., SHI, Y., WANG, L.-P., XIAO, Z., HE, X. T. & CHEN, S. 2011 Effect of shocklets on the velocity gradients in highly compressible isotropic turbulence. *Phys. Fluids* **23**, 125103.

WANG, J., SHI, Y., WANG, L.-P., XIAO, Z., HE, X. T. & CHEN, S. 2012 Effect of compressibility on the small scale structures in isotropic turbulence. *J. Fluid Mech.* **713**, 588–631.

WANG, J., WAN, M., CHEN, S. & CHEN, S. Y. 2018*a* Kinetic energy transfer in compressible isotropic turbulence. *J. Fluid Mech.* **841**, 581–613.

WANG, J., WAN, M., CHEN, S., XIE, C. & CHEN, S. Y. 2018*b* Effect of shock waves on the statistics and scaling in compressible isotropic turbulence. *Phys. Rev.* E **97**, 043108.

WANG, J., WANG, L.-P., XIAO, Z., SHI, Y. & CHEN, S. 2010 A hybrid numerical simulation of isotropic compressible turbulence. *J. Comput. Phys.* **229**, 5257–5259.

WANG, J., YANG, Y., SHI, Y., XIAO, Z., HE, X. T. & CHEN, S. 2013 Cascade of kinetic energy in three-dimensional compressible turbulence. *Phys. Rev. Lett.* **110**, 214505.

YEUNG, P. K., DONZIS, D. A. & SREENIVASAN, K. R. 2005 High-Reynolds-number simulation of turbulent mixing. *Phys. Fluids* **17**, 081703.

ZANK, G. P. & MATTHAEUS, W. H. 1990 Nearly incompressible hydrodynamics and heat conduction. *Phys. Rev. Lett.* **64**, 1243–1246.

ZANK, G. P. & MATTHAEUS, W. H. 1991 The equations of nearly incompressible fluids. I. Hydrodynamics, turbulence, and waves. *Phys. Fluids* A **3**, 69–82.